ORIGINAL RESEARCH

# A Highly Efficient One-for-All Nanodroplet for Ultrasound Imaging-Guided and Cavitation-Enhanced Photothermal Therapy

Dui Qin [1,2,*]
Lei Zhang [1,*]
Hongrui Zhu [1]
Junjie Chen [1]
Daocheng Wu [1]
Ayache Bouakaz [3]
Mingxi Wan [1]
Yi Feng [1]

[1]The Key Laboratory of Biomedical Information Engineering of Ministry of Education, Department of Biomedical Engineering, School of Life Science and Technology, Xi'an Jiaotong University, Xi'an, People's Republic of China; [2]Department of Biomedical Engineering, School of Bioinformatics, Chongqing University of Posts and Telecommunications, Chongqing, People's Republic of China; [3]UMR 1253, iBrain, Université de Tours, Inserm, Tours, F-37032, France

*These authors contributed equally to this work

Correspondence: Mingxi Wan; Yi Feng
The Key Laboratory of Biomedical Information Engineering of Ministry of Education, Department of Biomedical Engineering, School of Life Science and Technology, Xi' an Jiaotong University, Xi' An, 710049, People's Republic of China
Tel +86 29 82667924
Fax +86 29 82668668
Email mxwan@mail.xjtu.edu.cn;
fengyi@mail.xjtu.edu.cn

**Background:** Photothermal therapy (PTT) has attracted considerable attention for cancer treatment as it is highly controllable and minimally invasive. Various multifunctional nanosystems have been fabricated in an "all-in-one" form to guide and enhance PTT by integrating imaging and therapeutic functions. However, the complex fabrication of nanosystems and their high cost limit its clinical translation.

**Materials and Methods:** Herein, a high efficient "one-for-all" nanodroplet with a simple composition but owning multiple capabilities was developed to achieve ultrasound (US) imaging-guided and cavitation-enhanced PTT. Perfluoropentane (PFP) nanodroplet with a polypyrrole (PPy) shell (PFP@PPy nanodroplet) was synthesized via ultrasonic emulsification and in situ oxidative polymerization. After characterization of the morphology, its photothermal effect, phase transition performance, as well as its capabilities of enhancing US imaging and acoustic cavitation were examined. Moreover, the antitumor efficacy of the combined therapy with PTT and acoustic cavitation via the PFP@PPy nanodroplets was studied both in vitro and in vivo.

**Results:** The nanodroplets exhibited good stability, high biocompatibility, broad optical absorption over the visible and near-infrared (NIR) range, excellent photothermal conversion with an efficiency of 60.1% and activatable liquid-gas phase transition performance. Upon NIR laser and US irradiation, the phase transition of PFP cores into microbubbles significantly enhanced US imaging and acoustic cavitation both in vitro and in vivo. More importantly, the acoustic cavitation enhanced significantly the antitumor efficacy of PTT as compared to PTT alone thanks to the cavitation-mediated cell destruction, which demonstrated a substantial increase in cell detachment, 81.1% cell death in vitro and 99.5% tumor inhibition in vivo.

**Conclusion:** The PFP@PPy nanodroplet as a "one-for-all" theranostic agent achieved highly efficient US imaging-guided and cavitation-enhanced cancer therapy, and has considerable potential to provide cancer theranostics in the future.

**Keywords:** one-for-all nanodroplet, theranostics, photothermal therapy, acoustic cavitation, ultrasound imaging

## Introduction

Photothermal therapy (PTT) employs a photothermal conversion agent to convert near-infrared (NIR) laser energy into localized hyperthermia, resulting in a selective thermal ablation of cancer cells. As a promising approach for cancer therapy, it has received considerable attention due to its high controllability, minimal invasiveness, and negligible side–effects.[1–3] However, the challenges for its clinical applications include insufficient photothermal ablation, limited penetration depth and general

concerns regarding the fabrication and use of complex nanosystems in vivo.[4–7] To overcome such limitations, several nanosystems constructed with high efficient PTT agents that integrated multiple imaging modalities and therapeutic functions have attracted much attention recently.[1–7] As a promising theranostic agent, the NIR responsive perfluorocarbon (PFC) nanodroplets have been widely used for multimodal imaging guided PTT of tumors due to their ability of phase transition from nanodroplets to microbubbles.[8–17] During the PTT, the phase transition can be triggered by a localized hyperthermia, and the generated microbubbles in situ are effective contrast agents for ultrasound (US) imaging, which is an established non-invasive, low cost, and real-time imaging technique. Due to its intrinsic properties of phase transition and optical absorption, the NIR responsive PFC nanodroplet can also be used for combined photoacoustic (PA) and US imaging, and provide a strong increase in imaging sensitivity and specificity.[18–20] Moreover, it can carry a variety of extrinsic imaging agents at the same time, such as NIR dyes for fluorescence imaging,[8,10,13,16] or $Fe_3O_4$ nanoparticles for MRI imaging,[11] etc.

In addition to the advantage for multimodal imaging, the NIR responsive PFC nanodroplets have also been designed to improve the therapeutic outcomes by combining PTT with photodynamic therapy,[8,21] chemotherapy,[13,16] or radiotherapy,[22] etc. It has been reported that the combination of PTT and other therapies can achieve better therapeutic outcomes compared to PTT alone. When combined with US, acoustic cavitation of the microbubbles generated by nanodroplets vaporization would be triggered. The accompanied mechanical effects can enhance the PTT agents and/or drug delivery into deeper tumor regions by disrupting intratumoral barriers, consequently increasing the efficacy of PTT or photothermal–chemotherapy.[9,23,24] Considering that the acoustic cavitation can directly kill cancer cells due to serious cellular damage,[25–27] its combination with PTT is expected to act as an optional strategy for increasing PTT efficacy without encapsulating drug in the NIR responsive PFC nanodroplets.

The near-infrared responsive PFC nanodroplet usually has complex and delicate structures.[8–16] Nanosystems are typically fabricated using PFC as a core with a polymers/lipids shell, and PTT agents/drugs/genes embedded into the shell.[8–13] Alternatively, a hollow nanoparticle was prepared for PFC loading with conjugation/adsorption of PTT agents/drugs on its surface.[14–16] The majority have been constructed using an "all-in-one" approach, where

components that possess a single specific function (eg, PTT agent or imaging contrast agent) are combined with others, allowing multiple single components packaged in a single nanosystem.[28] The process of synthesis requires the addition of single functional moduli using a step-by-step approach and hence also requires multiple purification processes. Such lengthy and multistep synthesis and purification processes are relatively time-consuming, resulting in a lower yield and more difficulty of reproducibility, potentially limiting widespread clinical applications. Thus, it is anticipated that a simple but highly bioavailable theranostic agent could be prepared in a "one-for-all" approach, where a single component could serve multiple purposes.[28] Such an approach simplifies fabrication, avoids multiple synthetic steps, offering considerable promise for the future of nanomedicine.

In the present study, the low-boiling perfluoropentane (PFP) and the strong NIR-absorbing PPy were utilized to develop a theranostic core/shell-structured PFP@PPy nanodroplets using a "one-for-all" approach; then, a US imaging-guided and cavitation-enhanced cancer treatment strategy was proposed (Scheme 1). In the design, the PFP@PPy nanodroplets had a simple composition while maintaining multifunctionality as an efficient PTT agent, US contrast agent, and cavitation nucleus for cancer theranostics. Specifically, the PPy shell served both as a carrier for PFP and a PTT agent, while the PFP core was used as a US contrast agent and cavitation nucleus. Upon concurrent NIR laser and US irradiation, the photothermal effect of the PPy shells raised the local temperature and selectively ablated the cancer cells (ie, PTT); meanwhile, liquid-gas phase transition of the PFP cores occurred and generated microbubbles in situ. Heated regions where PFP microbubbles were generated and the extent of photothermal heating can be visualized via US imaging, suggesting that the strategy has great potential for PTT guidance and monitoring. Furthermore, acoustic cavitation was enhanced, and its mechanical effects acted on adjacent cancer cells causing cell death. Its combination with PTT significantly enhances the therapeutic efficacy against tumors. The photothermal effect and phase-transition of PFP@PPy nanodroplets, in addition to US imaging performance and acoustic cavitation of PFP microbubbles, were examined. The antitumor efficacy of the combined therapy and its potential mechanism were also studied both in vitro and in vivo. The strategy provides great potential for future cancer theranostic applications with the "one-for-all"-type PFP@PPy nanodroplets.
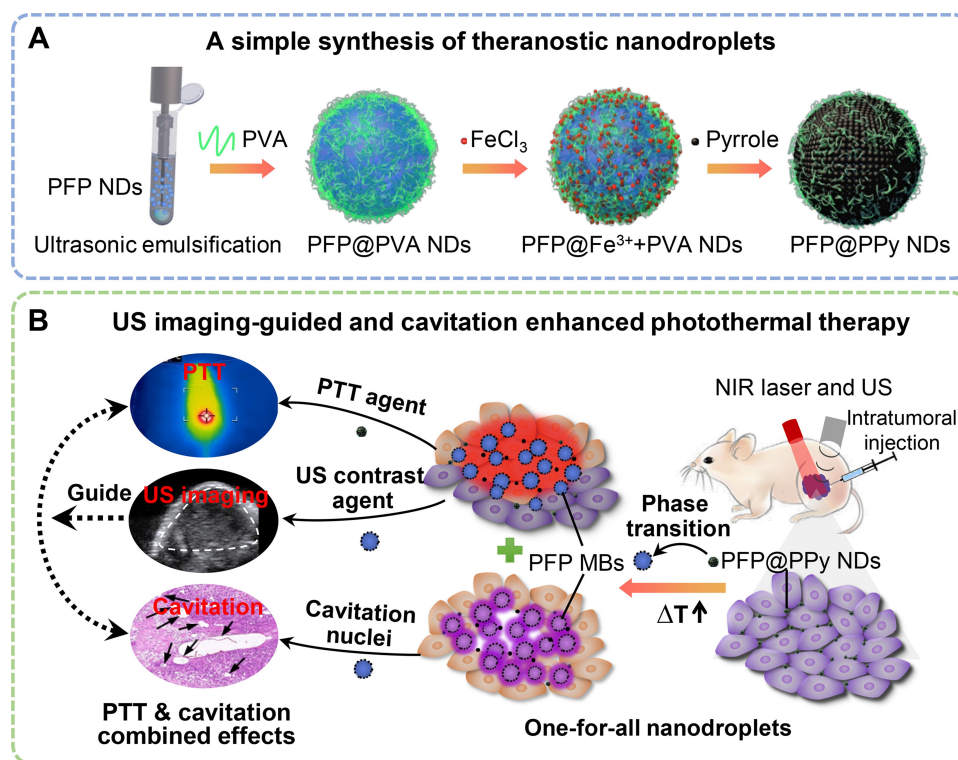
**Scheme 1** Schematic illustration showing (**A**) the synthetic process of "one-for-all"-type theranostic PFP@PPy NDs, and (**B**) corresponding mechanisms of US imaging-guided and cavitation-enhanced cancer therapy that combined photothermal and cavitation effects via the PFP@PPy NDs.

# Materials and Methods

## Materials

Perfluoropentane (PFP), polyvinyl alcohol (PVA, 31 kDa), pyrrole monomer, and propidium iodide (PI) were purchased from Sigma-Aldrich (USA). Iron (III) chloride was purchased from Aladdin Industry Corporation (Shanghai, China). All reagents were used as received without further additional treatment.

## Cell Culture and Animals

HeLa cervical cancer cells (CCL-2, ATCC, USA) were cultured in RPMI 1640 medium (HyClone, Thermo Scientific, USA) supplemented with 10% fetal bovine serum (HyClone, Thermo Scientific, USA) and 1% penicillin–streptomycin (Invitrogen, USA) in a humidified incubator at 37°C in an atmosphere containing 5% $CO_2$.

BALB/c nude mice (females, 4–6 weeks old) were purchased from Xi'an Jiao Tong University Laboratory Animal Center. All animal experiments were conducted in accordance with the institutional guidelines and were approved by the Animal Experimentation Ethics Committee of the School of Life Science and Technology of Xi'an Jiaotong University. A tumor model was established by administering $1\times10^7$ HeLa cells subcutaneously into the right flank of each nude mouse. Tumor size was measured using a caliper and the volume calculated by: Tumor volume = length $\times$ width$^2$/2.

## Synthesis and Characterization of the PFP@PPy Nanodroplets

PFP nanodroplets were prepared as described in a previous study.[27] Firstly, a 10 mL 3% v/v PFP emulsion was prepared by ultrasonic emulsification and then poured into a 4 mL 8% w/v polyvinyl alcohol (PVA) solution with stirring for 15 min in an ice bath. In situ oxidative polymerization was used to synthesize the PFP@PPy nanodroplets based on the formation of complexes between the PVA and ferric ion at the oil-water interface, in which PVA acted as a stabilizer and ferric ion acted as an oxidizing agent.[18] Briefly, 1 mL iron (III) chloride solution (FeCl₃, 300 mg/mL) was added to the PVA-emulsion and stirred for 30 mins, followed by the addition of 70 μL pyrrole monomer (Py). The reaction was continued in an ice bath for 4 h. Finally, the emulsion was centrifuged at 1000 g for 10 min to separate the PFP@PPy nanodroplets from

excess PPy nanoparticles (ie, those without a PFP core). The liquid supernatant was decanted and the concentrated precipitate resuspended in pure deionized water. The nanodroplets were washed three times by repeated centrifugation and resuspension. The PFP nanodroplets stabilized by the PVA were prepared as a control without the in situ oxidative polymerization.

The structural morphology of the PFP@PPy nanodroplets was evaluated by transmission electron microscopy (TEM, H-600, Hitachi Ltd., Japan). The size distribution was determined by dynamic light scattering (DLS, Malvern Instruments, Malvern, UK). Optical absorption spectra were measured using an ultraviolet-visible (UV-vis) spectrophotometer (T6, Purkinje General, China). To evaluate the cytotoxicity of the PFP@PPy nanodroplets, HeLa cells were incubated in 96-well plates with the nanodroplets at different volume concentrations of PFP (0.0002–0.02% v/v) for 24 h, and then a cell counting kit assay (CCK-8, Dojindo Laboratories, Japan) was used in accordance with the manufacturer's instructions. Specifically, after washing with culture medium, a 10% (v/v) CCK-8 solution was added to the culture medium and incubated for 2 h. The absorbance at 450 nm was measured using a microplate reader (SpectraMax 190, Molecular Devices, USA) and cell viability calculated as follows:

$$Cell\ viability(\%) = \frac{A_t - A_b}{A_c - A_b} \times 100\%$$

where $A_t$, $A_b$ and $A_c$ represented the absorbance of the treatment, blank (no cells), and control groups (cells without any treatment), respectively.

## In vitro Photothermal Effect and Hyperthermia-Induced Phase Transition of PFP@PPy Nanodroplets

The photothermal effect was investigated by placing a 0.2 mL aliquot of PFP@PPy nanodroplet suspension in the wells of a 96-well plate at various volume concentrations of PFP (0.001%-0.02% v/v) which were then irradiated for 10 mins using a NIR laser (808 nm, 1 W/cm$^2$, Hegel Radium Laser Technology Co., Ltd., China). The same volume of saline and 0.02% v/v PFP nanodroplets suspension acted as blank controls. Moreover, the photothermal effect of PFP@PPy nanodroplets (0.001% v/v) at different laser power densities (0.5, 1, 2, and 3 W/cm$^2$) was also evaluated. The temperature was measured using a thermocouple and recorded every 10

seconds. The photothermal conversion efficiency of PFP@PPy nanodroplets (0.002% v/v) exposed to the laser (1 W/cm$^2$, 10 min) was measured in accordance with Roper's method (the detailed calculation is presented in the Supporting Information).[29]

The liquid-gas phase transition of the PFP@PPy nanodroplets induced by laser irradiation was observed using an optical microscope (TiU, Nikon Instruments Inc., Japan). A drop of PFP@PPy nanodroplets (0.002% v/v) was placed on a glass slide and exposed to the NIR laser at 1 W/cm$^2$ for 5 min. During laser irradiation, the temperature was monitored every 20 seconds using an infrared thermal imaging camera (FLIR, USA).

## In vitro US Imaging and Acoustic Cavitation of Photothermal Microbubbles

To examine the US imaging performance of the photothermally generated microbubbles, a 2% agarose phantom was placed in a water tank containing a cylindrical hole (1 cm diameter, 1 cm depth) in which PFP@PPy nanodroplets (0.5 mL, 0.004% v/v) were poured. NIR laser (1 W/cm$^2$), US pulses (1 MHz, 2.2 MPa, 50 μs, and 10 Hz) or their combinations were applied for 1 min and NIR-induced hyperthermia, or its combination with negative US pressure was expected to trigger a phase transition of the PFP core and generate numerous photothermal microbubbles, as illustrated in Figure S1 (Supporting Information). All samples were then imaged with the same settings using a diagnostic US scanner (SonixTouch, Ultrasonix, Canada) in conventional B-mode and contrast-enhanced ultrasound (CEUS) mode (linear probe, 5 MHz, L14-5/38). The mean US intensity in the region of interest was determined by Image J software (NIH, http://rsb.info.nih.gov/ij/). Acoustic cavitation of the photothermal microbubbles was characterized by sonochemiluminescence (SCL) and passive cavitation detection (PCD) methods. The experimental system (Figure S2, Supporting Information) and procedures are presented in the supporting information. PFP nanodroplets alone represented the control group.

## Cell Viability Assay and Fluorescent Staining

To evaluate the therapeutic efficacy in vitro, HeLa cells were cultured in 96-well plates and randomly divided into three groups: no nanodroplets (0.9% saline), PFP nanodroplets, and PFP@PPy nanodroplets. Prior to treatment, 50 μL of each sample at a 0.002% volume concentration of

PFP was incubated with cells for 6 h. The samples were then submitted for 1 min to either the NIR laser (1 W/cm$^2$), US pulses (1 MHz, 2.2 MPa, 50 μs, and 10 Hz) or their combination (Figure S2, Supporting Information). Finally, the treated cells were incubated for 24 h and a CCK-8 assay used to examine cell viability, in accordance with the manufacturer's instructions.

Furthermore, live/dead fluorescent staining was also used to assess the status of treated cells. Prior to treatment, calcein-AM was added at a final concentration of 1 μM as a live-cell stain. After incubation for 15 min, propidium iodide (PI) was added as a dead cell stain to a final concentration of 20 μM. Calcein-AM crosses the cell membrane and is then converted to a membrane-impermeable and fluorescent form (excitation/emission: 488/520 nm) in living cells,[30] while PI can only pass through damaged cell membranes and undergoes dramatic fluorescence enhancement once bound to nucleic acids (excitation/emission of 535/617 nm). After treatment, a Digital Sight DSU2 camera (Nikon, Japan) connected to an inverted fluorescence microscope (TiU, Nikon, Japan) was used for fluorescent imaging.

## In vivo Evaluation of Enhanced US Imaging and Antitumor Effect

For US imaging in vivo, nude mice with a tumor volume of ~300 mm$^3$ were anesthetized using 1% pentobarbital sodium and divided into two groups (n = 3): (I) PFP@PPy nanodroplet and (II) PFP nanodroplet (control) groups. Firstly, US images of the tumors were captured using a diagnostic US scanner in conventional B-mode with a linear probe (15 MHz, L40-8/12). A 100 μL aliquot of nanodroplets was then injected intratumorally after which the tumors were irradiated with combined laser light and US pulses for 3 mins. Intratumoral injection has been extensively evaluated over recent decades[31–33] and it is possibly the best method to simulate the heterogeneous distribution of PTT agents.[33] Other parameters were the same as conducted in in vitro US imaging experiments. The mean US intensity of the tumors was measured in tumor regions. Infrared thermal images were recorded every 20 seconds to monitor variations in temperature in tumor regions.

To evaluate in vivo antitumor efficacy, mice with HeLa xenografts bearing tumors with a volume of ~100 mm$^3$ were divided into six groups (n = 5 in each): (I) Control, (II) PFP@PPy nanodroplets, (III) laser + US, (IV) PFP@PPy nanodroplets + US, (V) PFP@PPy nanodroplets + laser, (VI) PFP@PPy nanodroplets + laser + US. After intratumoral injection of a total of 100 μL of the respective sample, the various treatments were performed with laser irradiation (1.0 W/cm$^2$, 3 min), US pulses (1 MHz, 2.2 MPa, 50 μs, and 10 Hz, 3 min), or a combination of the two. Three days after treatment, a mouse in each group was chosen randomly and sacrificed, then the tumor tissues harvested for hematoxylin and eosin (H&E) staining to conduct pathological analysis. The tumor volume and body weight of each were monitored every other day for 14 days. The relative tumor volume (RTV) was calculated using the following formula:[34] RTV = (tumor volume on day t)/(tumor volume on day 0). The mice were sacrificed at the end of the experiment, and the tumors excised and weighed. Tumor inhibition rate (TIR) was calculated as follows: TIR = (1-mean tumor weight of treatment group/mean tumor weight of control group) × 100%.

## Statistical Analysis

Statistical analysis of the data was conducted using a two-sided Student's $t$-test. All data are expressed as means ± standard deviation from more than three repeated experiments. Differences were considered statistically significant for *$p$ < 0.05 and **$p$ < 0.01.

## Results and Discussion
### Characterization of PFP@PPy Nanodroplets

The synthesized PFP@PPy nanodroplets were spherical, uniform in size, and exhibited a distinct core-shell structure in TEM images (Figure 1A). Numerous PPy nanoparticles were evenly distributed on the surface, constituting a rough PPy shell. The results of DLS indicated that the nanodroplets had a mean diameter of 245 ± 13 nm with a narrow size distribution (Figure 1B), whereas for the PFP nanodroplets without PPy shells, the mean diameter was 194.8 ± 17 nm (Figure S3, Supporting Information). Furthermore, the mean diameter over 24 h at human physiological temperature was unchanged (Figure S4, Supporting Information), suggesting that the nanodroplets had high thermostability. It can be explained that the additional Laplace pressure experienced by the PFC nanodroplets may increase substantially its boiling temperature.[35,36] It has been reported that PFC nanodroplets with diameters of approximately 200 nm can passively accumulate around tumor tissues by virtue of the
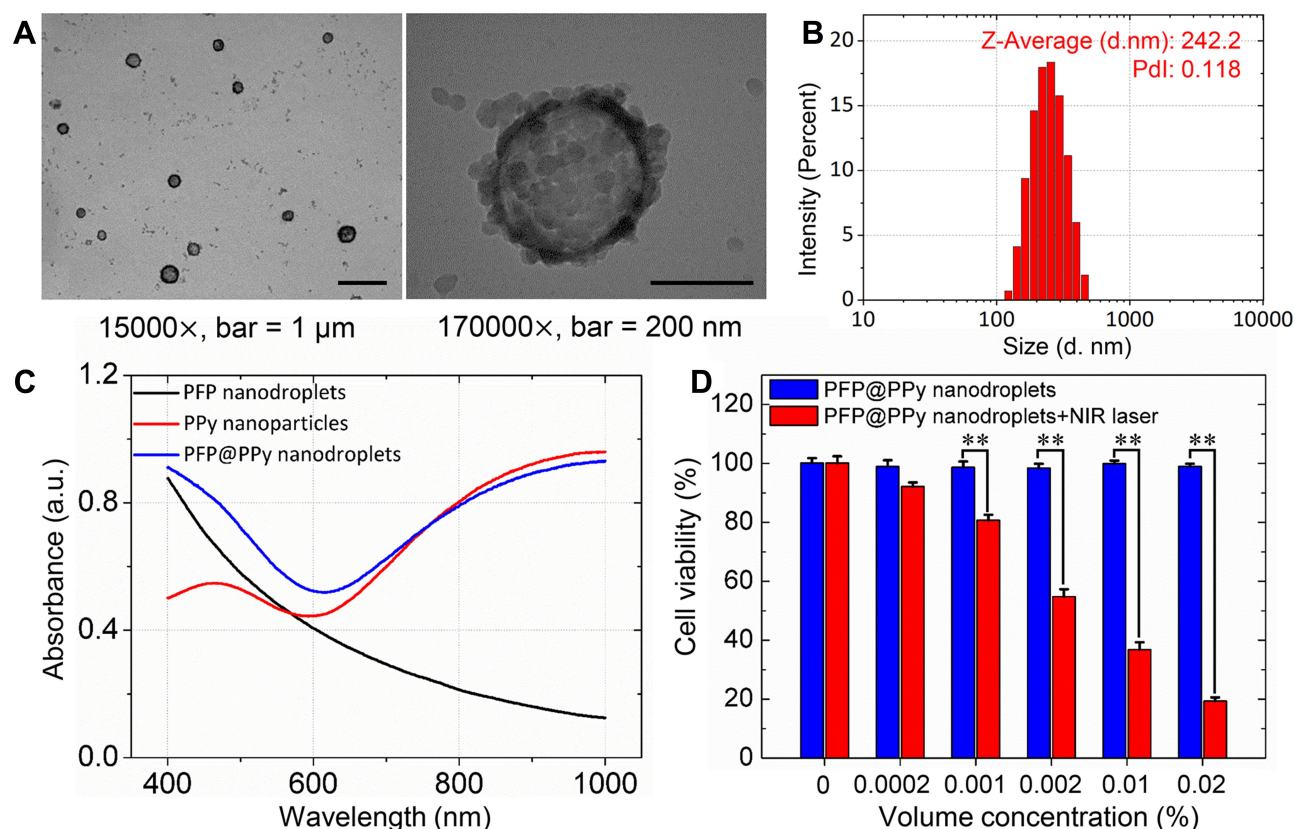
**Figure 1** Characterization of PFP@PPy nanodroplets. (**A**) TEM images. (**B**) The size distribution, determined by the DLS. (**C**) The absorption spectra of PFP nanodroplets, PPy nanoparticles and PFP@PPy nanodroplets. (**D**) Cytotoxicity of PFP@PPy nanodroplets at different volume concentrations with and without NIR laser irradiation. $**p < 0.01$.

enhanced permeability and retention (EPR) effect.[37,38] The data, therefore, strongly suggest that the PFP@PPy nanodroplets had appropriate size and stability suitable for additional in vivo theranostic applications.

The UV–vis absorbance spectra (from 400 to 1000 nm) shown in Figure 1C indicate that the PFP@PPy nanodroplets had strong and broad absorption extending from the UV to the NIR region, which is similar to the absorption spectra of PPy nanoparticles.[39–41] Also, the PFP nanodroplets showed to be successfully coated with a PPy shell, consistent with the TEM images. The apparent increase over the range 400–600 nm is likely caused by increased scattering from larger nanodroplets compared with the much smaller PPy nanoparticles.[18]

The PFP@PPy nanodroplets did not significantly inhibit cell proliferation at any concentrations in comparison with the control group (no nanodroplets), as shown in Figure 1D. This indicates that the PFP@PPy nanodroplets alone exhibited negligible cytotoxicity, possibly because of the biocompatibility of each component. When irradiated using a NIR laser (1 W/cm$^2$, 1 min), a significantly decreased cell

viability was observed at volume concentrations of PFP above 0.0002%, with cell viability decreasing with increasing volume concentration. The photothermal effect of PFP@PPy nanodroplets is responsible for the cell death, which increased with increasing nanodroplet concentration, consequently causing additional cell death.

## In vitro Photothermal Effect and Hyperthermia-Induced Phase Transition of PFP@PPy Nanodroplets

To evaluate the in vitro photothermal effect, temperature variations were monitored at different volume concentrations of PFP@PPy nanodroplets during NIR laser irradiation. As displayed in Figure 2A and B, no apparent temperature rise was observed in the 0.02% v/v PFP nanodroplets and saline groups, whereas the temperature of PFP@PPy nanodroplets increased rapidly with the maxima proportional to nanodroplet concentration and power density of the incident laser light. Specifically, the temperature of the 0.02% v/v PFP@PPy nanodroplets increased by 41.9°C after 10 mins laser irradiation, but

by only 8.9°C and 5.4°C for the PFP nanodroplets and saline, respectively. The results suggest that the principal photothermal effect of the PFP@PPy nanodroplets could be attributed to the optical absorption of the PPy shell, its heating effect evidently dependent on nanodroplet concentration and laser power density.[39–41] Furthermore, as shown in Figure 2C and S5 (Supporting Information), photothermal conversion efficiency of the PFP@PPy nanodroplets was assessed to be 60.13%, as presented in the Supporting Information. The strong absorbance and excellent photothermal conversion efficiency of PFP@PPy nanodroplets in the NIR window are beneficial to treat deeper tumours via PTT and improve treatment outcomes.

Due to the photothermal effect, the PFP@PPy nanodroplets underwent a liquid-gas phase transition, as observed by microscope after 0, 1, 3, and 5 mins during NIR laser irradiation. As displayed in Figure 2D, a few photothermal microbubbles were gradually generated after 1 min (~50.3°C), the number distinctly increased after 3 mins at a temperature of approximately 57.9°C.

Finally, the microbubbles started to disappear at higher temperatures (~62.1°C). In contrast, the PFP nanodroplets without PPy shells did not generate any photothermal microbubbles during laser irradiation. The results demonstrate that the photothermal effect of the PPy shells elevated the local temperature and subsequently triggered a liquid–gas phase transition of the PFP core to generate numerous microbubbles. According to previous studies,[14,15,34,42–44] the photothermally generated microbubbles acted as a US contrast agent, thus achieving a significant enhancement of US imaging, suitable for US imaging-guided PTT of tumors. More importantly, they could also act as cavitation nuclei to enhance acoustic cavitation activity[18] and further improve therapeutic efficacy against tumors through cavitation-mediated sonoporation with concurrent US application.[23,24] Therefore, US imaging performance and acoustic cavitation of the photothermally generated microbubbles from the PFP@PPy nanodroplets were investigated in the following section.
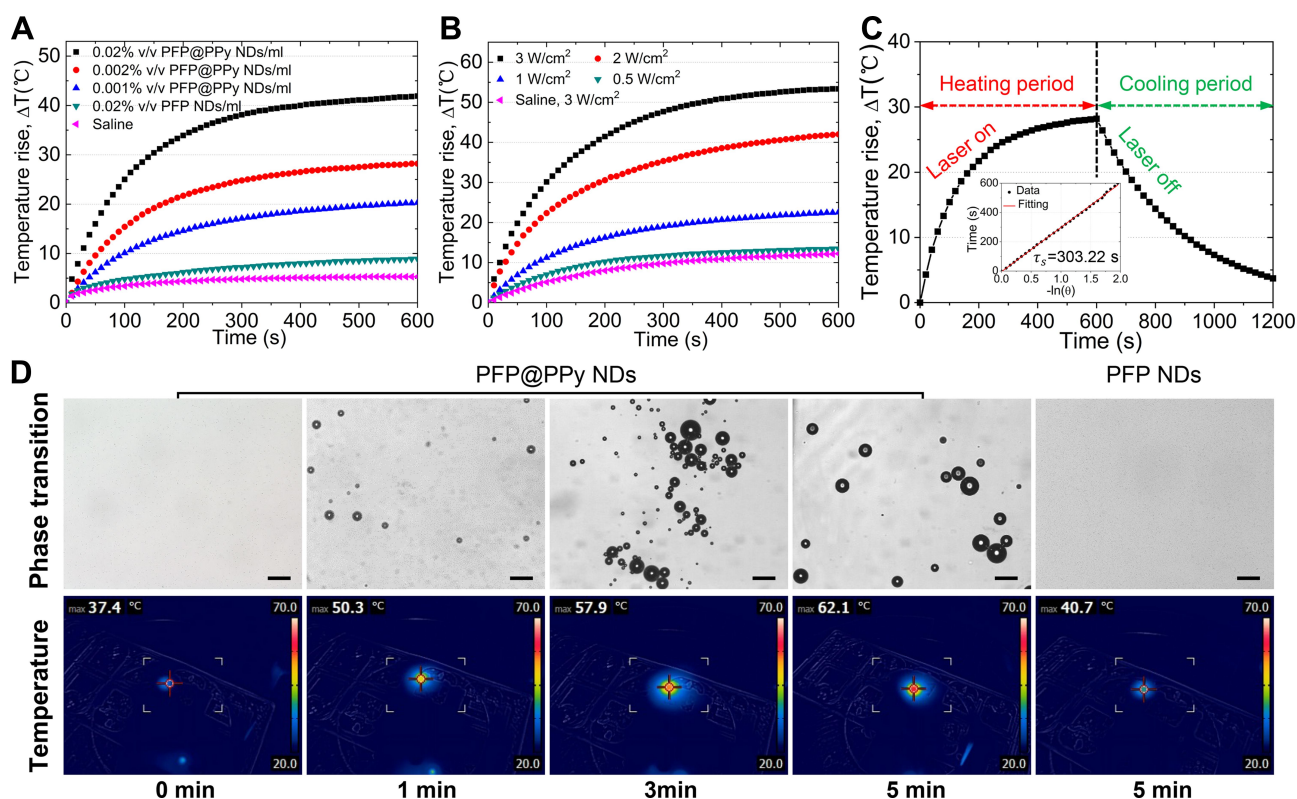


**Figure 2** Photothermal temperature curves of PFP@PPy nanodroplets over time (0-10 min) with (**A**) different volume concentrations (NIR laser: 1 W/cm²) and (**B**) different laser power densities (volume concentration of PFP: 0.001% v/v). (**C**) Photothermal conversion efficiency of PFP@PPy nanodroplets. (**D**) The liquid-gas phase transition of PFP@PPy nanodroplets (volume concentration of PFP: 0.002% v/v) was evaluated using microscopic (upper) and IR thermal images (lower) under laser irradiation (1 W/cm²) at different time points. The same concentration of PFP nanodroplets were used as the control group. Scale bar = 10 μm.

# In vitro US Imaging Performance and Acoustic Cavitation Activity of Photothermal Microbubbles

The US imaging capability of the photothermally generated microbubbles (Figure 2D) with NIR laser irradiation was evaluated in vitro to confirm the potential of PFP@PPy nanodroplets as a US contrast agent for US imaging-guided PTT of tumors. As shown in Figure 3A, the B-mode and CEUS images of the PFP@PPy nanodroplet groups were clearly enhanced after either laser irradiation alone (group I) or the combination of laser and US irradiation (group II). In comparison, no apparent echogenicity/contrast enhancement was observed in the PFP nanodroplet groups (control groups III and IV). Notably, when laser and US irradiation were combined, it was speculated that the onset of nanodroplet vaporization might be triggered by the combination of hyperthermia in the PFP core from the photothermal effect of the PPy shell and negative pressure from the acoustic rarefaction phase, in accordance with previous studies.[18,23,24] However, there were no apparent echogenicity/contrast changes in both PFP@PPy nanodroplets and PFP nanodroplets groups as ultrasound was irradiated alone (Figure S6, Supporting Information). Here, the ultrasound cannot trigger the vaporization of nanodroplet due to its low acoustic pressure, which is beneficial to avoid the undesirable damage caused by the high acoustic pressures. The

mean US signal intensities in B-mode and CEUS mode were calculated by Image J software, as presented in Figure 3B and C, respectively. Under the same irradiation conditions, mean US intensity values in B-mode and CEUS mode both increased significantly compared with the corresponding control groups. Overall, the results indicate that the PFP@PPy nanodroplets, which displayed excellent gas microbubble-generation performance in response to either NIR laser or combined laser and US irradiation, are excellent US contrast agents for US imaging-guided PTT of cancer.

For concurrent laser and US irradiation, the photothermally generated microbubbles could also act as cavitation nuclei that enhance acoustic cavitation and cavitation–mediated cancer therapy.[18,23,24] Firstly, the acoustic cavitation region was visualized by SCL. Using the same irradiation conditions, the SCL images displayed an elliptical luminous region when PFP@PPy nanodroplets were used (group I), while no light generated in the control group II (PFP nanodroplets), as shown in Figure 4A and B. This suggests that the generation of microbubbles played a critical role in manifesting active acoustic cavitation. PCD methods were also used to characterize bubble cavitation, as presented in Figure 4C and D, indicating that the recorded acoustic cavitation emissions in the PFP@PPy nanodroplets had larger amplitudes, with significant increase in harmonic components (2, 3, and 4 MHz) and broad
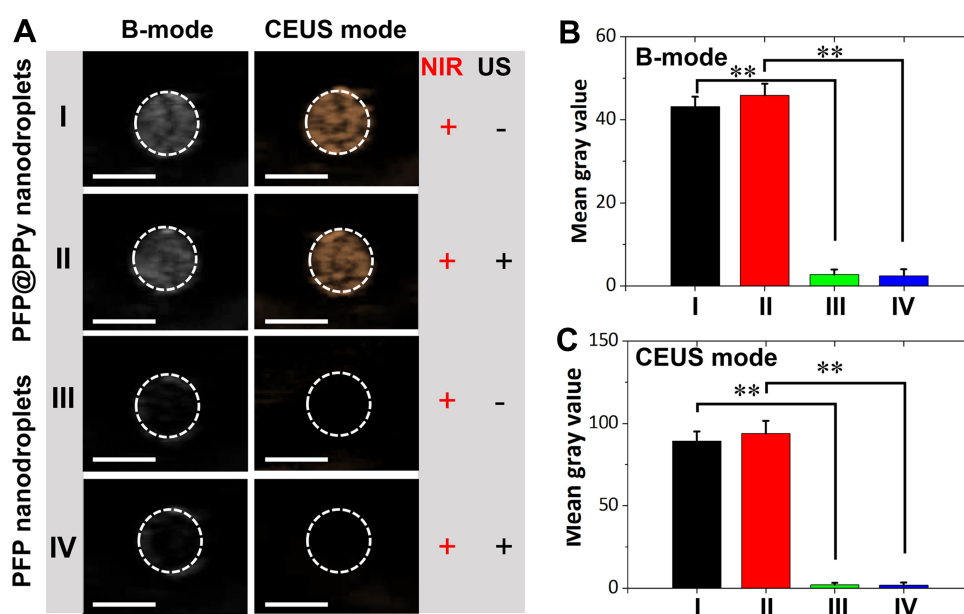


**Figure 3** In vitro US imaging performance. (**A**) B-mode and contrast enhanced ultrasound (CEUS) imaging of PFP@PPy nanodroplets after NIR laser irradiation (1 W/cm$^2$) or combined laser and US irradiation (1 MHz, 2.2 MPa, 50 μs and 10 Hz) for 1 min in gel phantoms. The same concentration of PFP nanodroplets were used as negative controls. The mean US intensity values in both (**B**) B-mode and (**C**) CEUS mode images. **$p < 0.01$. Scale bar = 1 cm.

acoustic emissions, compared with the PFP nanodroplets alone. According to previous studies,[45,46] stable and inertial cavitation is characterized by harmonic components and broad band acoustic emissions, respectively. Therefore, it strongly suggests that both stable and inertial cavitation occurred with the combination of laser and US irradiation of PFP@PPy nanodroplets.

The mechanical bioeffects of bubble cavitation may cause damage to adjacent cells, leading to changes in membrane permeability or cell death from irreversible damage, and consequently improve tumor therapeutic efficacy.[25–27] Note that the microbubbles would be destroyed during inertial cavitation, but there was no apparent decrease in echogenicity/contrast after US application (group II in Figure 3). It indicated that a balance might be achieved between the cavitation-induced microbubble destruction and more microbubble generation due to the contribution of additional US to nanodroplet vaporization. Considering that the generated

microbubbles from the phase transition of PFP@PPy nanodroplets can result in apparent enhancement of both US imaging (Figure 3) and acoustic cavitation (Figure 4), PFP@PPy nanodroplets with combined laser and US irradiation is likely to show considerable potential in US imaging-guided and cavitation-enhanced PTT for precise and highly efficient combined therapy of cancer.

## In vitro Enhanced Cancer Therapy with Combined Photothermal and Cavitation Effects

To evaluate the enhanced therapeutic efficacy of PTT with simultaneous microbubble cavitation during combined laser and US irradiation, HeLa cells were incubated with PFP@PPy nanodroplets and irradiated with either NIR laser, US, or both, and then cell viability was evaluated using a CCK-8 assay and live/dead cell fluorescent staining.
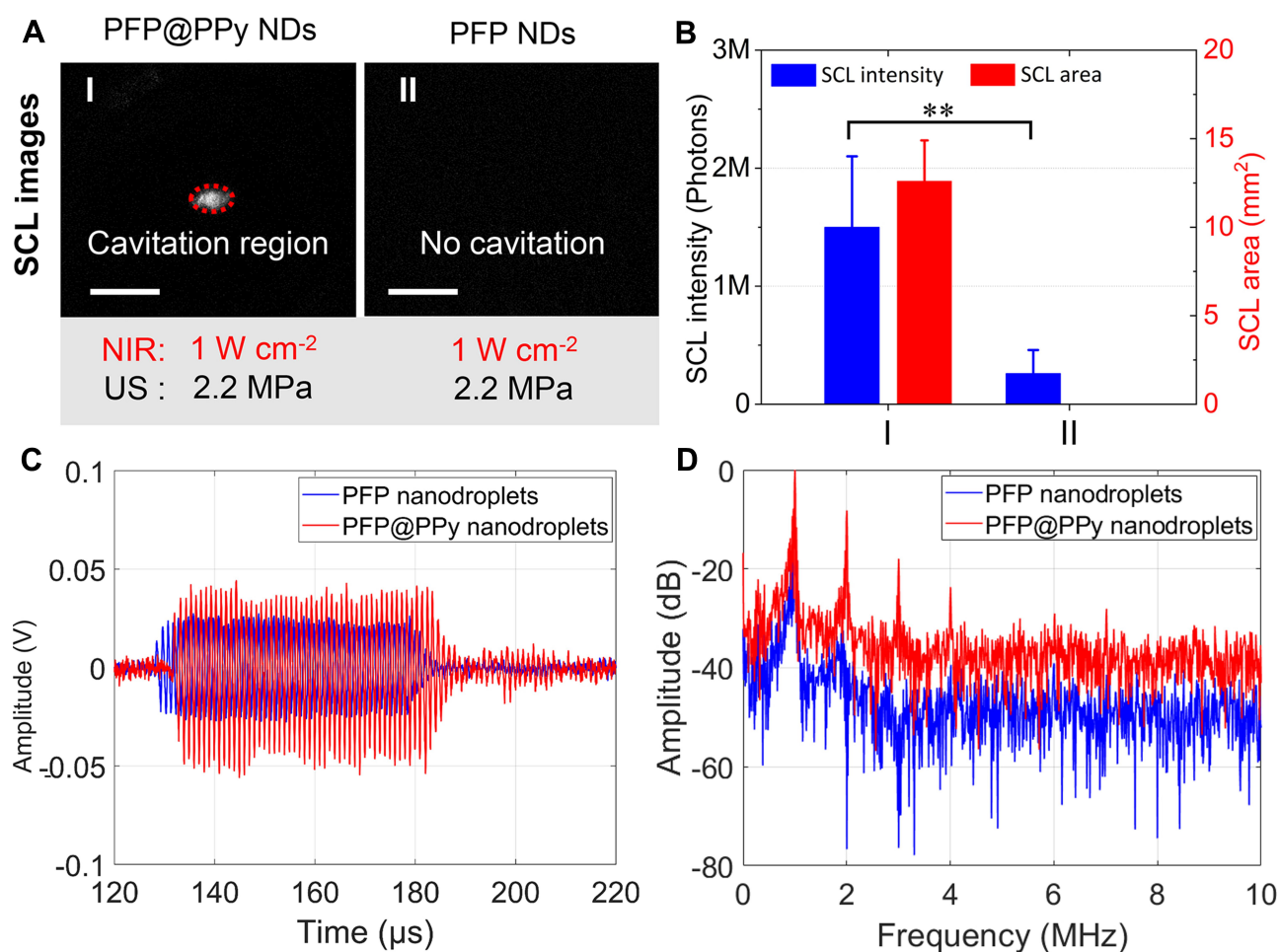


**Figure 4** Characterization of the acoustic cavitation of photothermally generated microbubbles under combined NIR laser (1 W/cm²) and US (1 MHz, 2.2 MPa, 50 μs and 10 Hz) irradiation. (**A**) The pictures of the SCL regions in two groups and (**B**) corresponding light intensities and luminous areas. Passive acoustic detection (PCD) of cavitation events, including (**C**) time-domain signals and (**D**) frequency spectrum analysis. **\*\*p < 0.01. Scale bar = 1 cm.

The quantitative evaluation of the cell viability after different treatments is shown in Figure 5. In the groups of only cells (no nanodroplets) and PFP nanodroplets alone, no significant decrease in cell viability was observed for all irradiation conditions. However, a significant decrease of cell viability of 58.3±5.4% was observed after the cells were treated with PFP@PPy nanodroplets and laser irradiation, presumably attributed to the photothermal effect of the PFP@PPy nanodroplets. When laser irradiation was combined with US application, cell viability significantly decreased to 18.9 ± 4.9%, compared with either energy modality alone (laser: 58.3 ± 5.4% or US: 97.6 ± 2.1%). It clearly indicates that the acoustic cavitation significantly enhanced the PTT efficacy with the assistance of PFP@PPy nanodroplets under the combined laser and US irradiation.

To further elucidate the mechanism of the combined effects, fluorescent staining and bright-field microscopic images of the four groups were presented, as shown in Figure 6A. When laser and US irradiation were combined (group I), fluorescent staining with calcein-AM (green) and PI (red) showed that almost all cells died, whereas no apparent cell death was observed in the PFP nanodroplet group (IV, control group). It demonstrated that the PPy shell of the PFP@PPy nanodroplets is critical for effective cancer cell death due to the excellent photothermal effects of the PPy shell (Figure 2A–C). Partial dead cells were observed under laser irradiation alone (group II), while no obvious dead cells were found under US irradiation alone
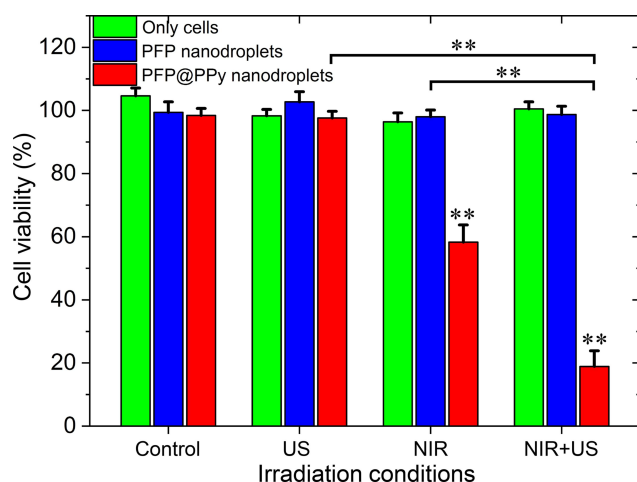
(group III). This suggests that the laser-induced photothermal effect of the PPy shell contributed to the observed cell death, but US application alone did not induce sufficient damage to kill the cancer cells. Furthermore, low calcein and high PI fluorescence intensity values also confirmed a significant increase in cell death following treatment of the cells with combined laser and US irradiation (Figure 6B), as compared with either laser or US application alone. More importantly, apparent cell detachment and numerous photothermal microbubbles were only observed in group I, as displayed in bright-field microscopy images. In addition, cell detachment was also verified by quantitative analysis of the live/dead cell number. This indicated a significant decrease in the total number of cells (approximately a 21% decrease compared with the control group) only in group I, as shown in Figure 6C. It is known that the mechanical effects of cavitation can cause cell death and cell detachment in cancer therapy.[47,48] Hence, intense acoustic cavitation during combined laser and US irradiation, as revealed by the SCL image in Figure 6D, was responsible for significantly increased cell death and detachment. Overall, these results demonstrate that the mechanism of combined therapy operates at the cellular level. Specifically, the photothermal effect of the PPy shell caused local hyperthermia for photothermal ablation of cancer cells and simultaneously triggered photothermal microbubbles generation. As cavitation nuclei, these microbubbles significantly increased acoustic cavitation activity and the accompanied mechanical effects destroyed adjacent cancer cells, eventually achieving acoustic cavitation-enhanced PTT of tumors.

## In vivo Evaluation of the Enhanced US Imaging and Antitumor Effects

Encouraged by in vitro US imaging performance of photothermal microbubbles (Figure 3), in vivo US imaging performance was investigated in HeLa–bearing BALB/c mice. As shown in Figure 7A, the tumor site in mice displayed no apparent enhancement in US signal after combined laser and US irradiation for 3 mins following the injection of PFP nanodroplets (group I), whereas for the PFP@PPy nanodroplet group (II), the tumor exhibited clear US imaging enhancement. Additionally, quantitative analysis also demonstrated that the mean US intensity in PFP@PPy nanodroplets was significantly higher than the PFP nanodroplets group (Figure 7B). According to previous studies,[14,15,34,42–44] PFP@PPy nanodroplets acting as US
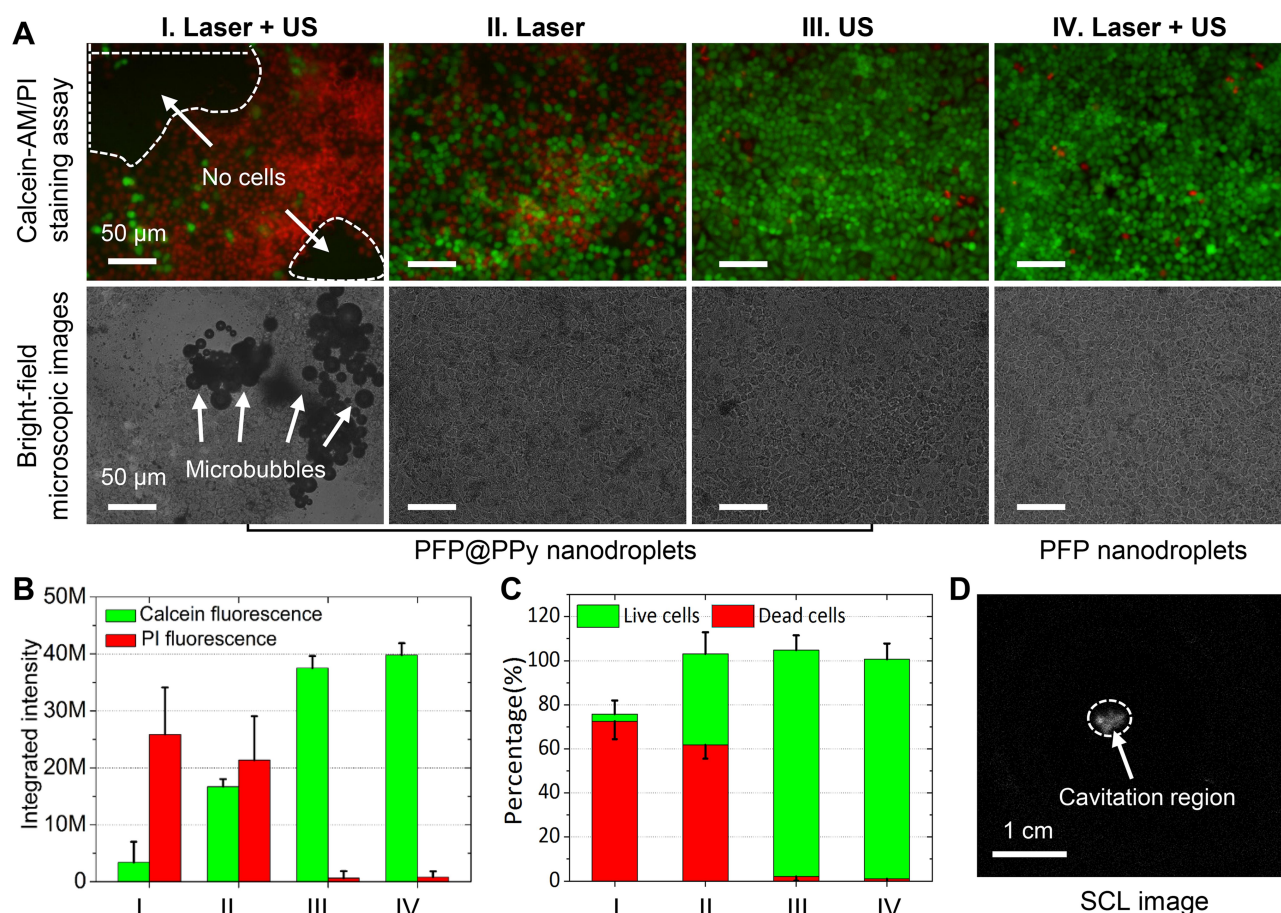


**Figure 5** In vitro evaluation of therapeutic efficacy after various treatments by using cell-counting kit-8 (CCK-8) assay. The cultured cells were randomly divided into three groups, including the cells without nanodroplets, with PFP nanodroplets and PFP@PPy nanodroplets at the same volume concentration of PFP (0.002% v/v). **$p$ < 0.01.

**Figure 6** (**A**) The merged calcein-AM/PI staining fluorescent and bright-field microscopic images at different experimental conditions. (**B**) The quantitative analysis of integrated calcein and PI fluorescence in the cells. (**C**) The relative number of live/dead cells at different conditions. (**D**) The SCL representative image of the group I for characterizing the acoustic cavitation.

contrast agents in vivo can be explained by the phase transition of PFP cores triggered by PTT to generate numerous photothermal microbubbles, as displayed in Figure 2D. Furthermore, this was also verified by the elevated tumor

surface temperature, as monitored by infrared thermal images (Figure S7, Supporting Information). There was a rapid and substantial temperature increase to ~50°C in the PFP@PPy nanodroplet group (Figure S8, Supporting
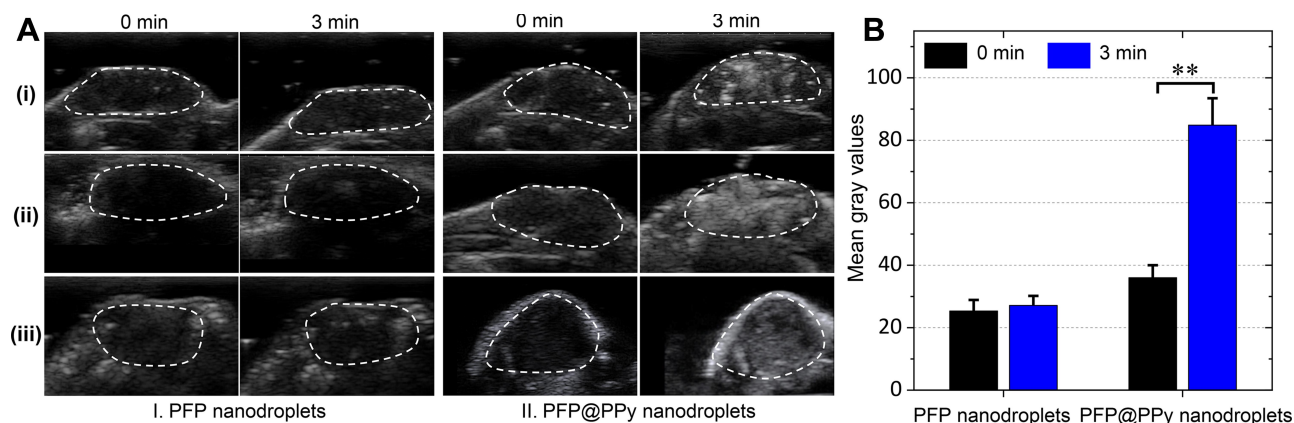


**Figure 7** (**A**) In vivo US images of tumors before and after the combined laser and US irradiation with (I) PFP nanodroplets (control group) and (II) PFP@PPy nanodroplets (n = 3). White dashed circles indicate the region of tumors. (**B**) In vivo mean US intensity values of the two groups. **$p < 0.01$.

Information). The results demonstrate that the PFP@PPy nanodroplets possessed enhanced US imaging capability in vivo, which is of great importance for US imaging-guided photothermal cancer therapy.

The photothermal effect of the PFP@PPy nanodroplets caused a local temperature rise (Figures S7 and S8, Supporting Information), triggering photothermal microbubble generation for US imaging enhancement (Figure 7A) and thermally ablating cancer cells in vivo. Furthermore, the generated photothermal microbubbles also acted as cavitation nuclei that increased acoustic cavitation activity (Figure 4) during the combined laser and US irradiation. The mechanical bioeffects of bubble cavitation also caused adjacent cancer cell death and significantly enhanced the PTT of cancer cells (Figure 5). Therefore, the antitumor efficacy of the combined therapy was evaluated, combining photothermal and cavitation effects in vivo in tumor–bearing mice.

As shown in Figure 8A and S9 (Supporting Information), a sharp increase in tumor volume was clearly observed over 14 days in groups I-IV, with treatment by saline only (control, I), PFP@PPy nanodroplets (II), laser + US (III) and PFP@PPy nanodroplets + US (IV), respectively. There was no significant difference between the groups, indicating that PFP@PPy nanodroplets alone, combination of laser and US in absence of PFP@PPy nanodroplets or PFP@PPy nanodroplets with US application alone did not cause potentially destructive effects and exhibited only negligible antitumor efficacy. When the PFP@PPy nanodroplets were irradiated by laser (group V), a substantial slower tumor growth was observed compared with the control group, probably due to the photothermal ablation of tumor cells assisted with PFP@PPy nanodroplets. The observed anticancer effects might be overestimated because intratumoral injection can increase the concentrations of PFP@PPy nanodroplets at the target site. However, it seems that two tumors treated with PTT alone recurred after 8 d, indicating incomplete eradication of tumor cells, limited by the shallow and uneven hyperthermia during single PTT.[49,50] Most notably, the treatment of PFP@PPy nanodroplets with combined laser and US irradiation (group VI) demonstrated the strongest inhibition of tumor growth. This strongly suggests that combined photothermal ablation and cavitation-mediated cell destruction exerts a significantly enhanced antitumor effect in vivo.

The tumors were dissected and weighed (Figure 8B and C) at day 14, where tumor size and weight were found to be
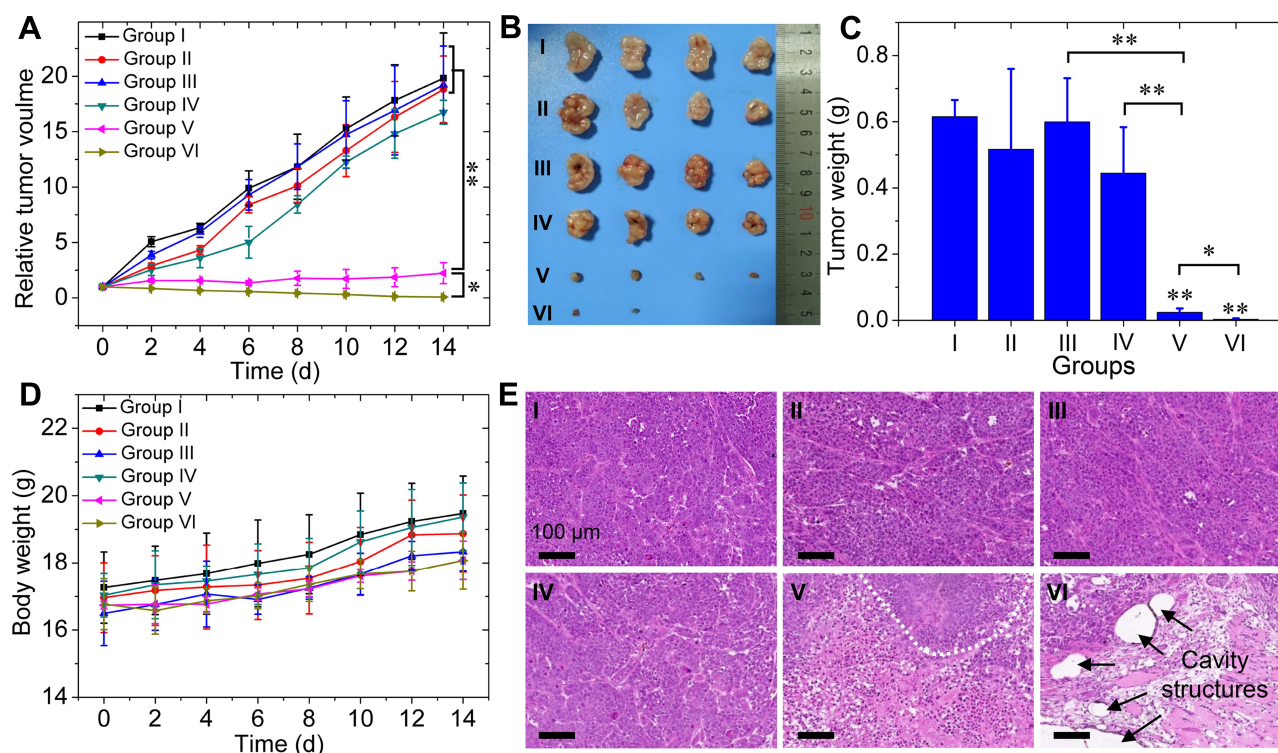


**Figure 8** In vivo antitumor efficacy. (**A**) Time-dependent tumor growth curves after treatment (n = 4). (**B**) The photographs and (**C**) the mean tumor weight of the excised tumors from different groups. (**D**) Time-dependent body weight curves of nude mice after different treatments. (**E**) Representative images of H&E-stained tumor sections showing pathological changes. (Groups I) Saline, II: PFP@PPy nanodroplets, III: laser + US, IV: PFP@PPy nanodroplets + US, (V) PFP@PPy nanodroplets + laser, VI: PFP@PPy nanodroplets + laser + US).*$p < 0.05$,**$p < 0.01$.

significantly reduced in groups V and VI. Compared with group V, mean tumor weight of group VI was 8.7-fold smaller, very close to zero. It also demonstrates that combined therapy resulted in a higher tumor inhibition rate (99.5%) than PTT alone. In addition, the bodyweight of each treated mouse was recorded at the target day and there was no significant change in body weight of mice in any group throughout the course of treatment (Figure 8D).

Histological analysis of tumor tissues by H&E staining was conducted, as shown in Figure 8E. Groups I to IV displayed intact nuclear morphology, indicating negligible cell apoptosis or necrosis. Thus, the PFP@PPy nanodroplets (group II) and laser + US irradiation (group III) can be considered as safe. There was also no evidence of cancer cell lysis/death using US irradiation alone (group IV). However, the tumor cells were severely damaged by treatment with PFP@PPy nanodroplets and laser irradiation alone (group V) or combined laser and US irradiation (group VI). Additionally, in group VI, considerable cavity structures were observed in the tumor tissue, as displayed by arrows, whereas no apparent cavity structures were observed in group V. The results suggest that the mechanical forces from bubble cavitation during US stimulation (such as cavitation-associated shear stress, shock waves, or microjets[25,51,52]) destroyed adjacent tumor tissue and caused the generation of cavity structures, consistent with in vitro cell experiments (Figure 6).

In vitro and in vivo experiments demonstrated that the PFP@PPy nanodroplets combined with NIR laser and US irradiation exhibited an excellent antitumor effect. This can be attributed to the following reasons. Firstly, excellent photothermal conversion efficiency of PPy shells caused an increase in local temperature (Figure 2, S7, and S8, Supporting Information) under laser irradiation and resulted in PTT of the cancer cells (Figures 5, 6, and 8E). Secondly, the photothermally generated microbubbles enhanced acoustic cavitation (Figures 4 and 6D), their mechanical effects are able to destroy adjacent cancer cells and cause cell death (Figures 6A and 8E). Thus, the combination of PTT and cavitation-mediated cell destruction significantly improved the therapeutic outcomes as compared to the PTT alone (Figures 5, 6 and 8).

## Conclusion

A "one-for-all" theranostic PFP@PPy nanodroplet with low-boiling PFP as the core and PPy that exhibited broad optical absorption constituting the shell was successfully constructed. The PFP@PPy nanodroplets represent an efficient PTT agent with outstanding photothermal conversion properties that can efficiently transfer NIR light into local hyperthermia for photothermal ablation of tumors. Meanwhile, the liquid-gas phase transition of the PFP cores was also triggered to generate numerous photothermal microbubbles, acting as excellent US contrast agents and cavitation nuclei as confirmed by the significant enhancement in the US imaging and acoustic cavitation. Furthermore, antitumor therapy displayed a significant increase in cell death, cell detachment in vitro, and inhibition of tumor growth in vivo than using either a laser or US alone. This finding strongly suggests that combined photothermal ablation and cavitation-mediated cell destruction contributed to cancer cell death, subsequently resulting in higher antitumor efficacy, with a tumor inhibition rate of up to 99.5%. Hence, the one-for-all theranostic PFP@PPy nanodroplet exhibited multiple capabilities, acting as a PTT agent, US contrast agent, and cavitation nucleus for US imaging-guided cavitation-enhanced PTT of tumors, representing a promising approach for high efficiency cancer theranostics.

## Abbreviations

PTT, photothermal therapy; PFP, perfluoropentane; PPy, polypyrrole; PFP@PPy NDs, perfluoropentane nanodroplets with polypyrrole shells; US, ultrasound; NIR, near-infrared; PA, photoacoustic; PFC, perfluorocarbon; EPR, enhanced permeability and retention; PVA, polyvinyl alcohol; PI, propidium iodide; Py, pyrrole monomer; TEM, transmission electron microscope; DLS, dynamic light scattering; UV-vis, ultraviolet-visible; CCK-8, cell counting kit; CEUS, contrast-enhanced ultrasound; SCL, sonochemiluminescence; PCD, passive cavitation detection; H&E, hematoxylin and eosin; RTV, relative tumor volume; TIR, tumor inhibition rate.

## Acknowledgments

## Disclosure

The authors report no conflicts of interest in this work.

# References

1. Zou L, Wang H, He B, et al. Current approaches of photothermal therapy in treating cancer metastasis with nanotherapeutics. *Theranostics*. 2016;6(6):762–772. doi:10.7150/thno.14988

2. Hu JJ, Cheng YJ, Zhang XZ. Recent advances in nanomaterials for enhanced photothermal therapy of tumors. *Nanoscale*. 2018;10 (48):22657–22672. doi:10.1039/C8NR07627H

3. Wang J, Wu X, Shen P, et al. Applications of inorganic nanomaterials in photothermal therapy based on combinational cancer treatment. *Int J Nanomedicine*. 2020;15:1903–1914. doi:10.2147/IJN.S239751

4. Liu Y, Bhattarai P, Dai Z, Chen X. Photothermal therapy and photo-acoustic imaging via nanotheranostics in fighting cancer. *Chem Soc Rev*. 2019;48(7):2053–2108.

5. Hu Q, Huang Z, Duan Y, Fu Z, Bin L. Reprogramming tumor microenvironment with photothermal therapy. *Bioconjugate Chem*. 2020;31(5):1268–1278. doi:10.1021/acs.bioconjchem.0c00135

6. Li X, Lovell JF, Yoon J, Chen X. Clinical development and potential of photothermal and photodynamic therapies for cancer. *Nat Rev Clin Oncol*. 2020;17(11):657–674. doi:10.1038/s41571-020-0410-2

7. Shramova EI, Kotlyar AB, Lebedenko EN, Deyev SM, Proshkina GM. Near-infrared activated cyanine dyes as agents for photothermal therapy and diagnosis of tumors. *Acta Naturae*. 2020;12(3):102–113. doi:10.32607/actanaturae.11028

8. Chen S, Huang B, Pei W, et al. Mitochondria-targeting oxygen-sufficient perfluorocarbon nanoparticles for imaging-guided tumor phototherapy. *Int J Nanomedicine*. 2020;15:8641–8658. doi:10.2147/IJN.S281649

9. Hu Y, Xue S, Long T, et al. Opto-acoustic synergistic irradiation for vaporization of natural melanin-cored nanodroplets at safe energy levels and efficient sono-chemo-photothermal cancer therapy. *Theranostics*. 2020;10(23):10448–10465. doi:10.7150/thno.44879

10. Liang Y, Yang H, Li Q, et al. Novel biomimetic dual-mode nano-droplets as ultrasound contrast agents with potential ability of precise detection and photothermal ablation of tumors. *Cancer Chemother Pharmacol*. 2020;86(3):405–418. doi:10.1007/s00280-020-04124-x

11. Xu Y, Li W, Chen S, et al. Near-infrared responsive phase-shifted nanoparticles for magnetically targeted MR/US imaging and photo-thermal therapy of cancer. *Front Bioeng Biotechnol*. 2020;8(1322). doi:10.3389/fbioe.2020.599107.

12. Zhu J, Wang Z, Xu X, et al. Polydopamine-encapsulated perfluoro-carbon for ultrasound contrast imaging and photothermal therapy. *Mol Pharm*. 2020;17(3):817–826. doi:10.1021/acs.molpharmaceut.9 b01070

13. Sheng D, Deng L, Li P, Wang Z, Zhang Q. Perfluorocarbon nano-droplets with deep tumor penetration and controlled drug delivery for ultrasound/fluorescence imaging guided breast cancer therapy. *ACS Biomater Sci Eng*. 2021;7(2):605–616. doi:10.1021/acsbiomaterial s.0c01333

14. Jia X, Cai X, Chen Y, et al. Perfluoropentane-encapsulated hollow mesoporous Prussian blue nanocubes for activated ultrasound ima-ging and photothermal therapy of cancer. *ACS Appl Mater Interfaces*. 2015;7(8):4579–4588. doi:10.1021/am507443p

15. Ren J, Zhang L, Zhang J, et al. Light-activated oxygen self-supplied starving therapy in near-infrared (NIR) window and adjuvant hyperthermia-induced tumor ablation with an augmented sensitivity. *Biomaterials*. 2020;234:119771. doi:10.1016/j.biomaterials.20 20.119771

16. Zhang J, Huang H, Xue L, et al. On-demand drug release nanoplat-form based on fluorinated aza-BODIPY for imaging-guided chemo-phototherapy. *Biomaterials*. 2020;256:120211. doi:10.1016/j. biomaterials.2020.120211

17. Li Y, Lu J, Zhang J, et al. Phase-change nanotherapeutic agents based on mesoporous carbon for multimodal imaging and tumor therapy. *ACS Appl Bio Mater*. 2020;3(12):8705–8713. doi:10.1021/ acsabm.0c01102

18. Li DS, Yoon SJ, Pelivanov I, et al. Polypyrrole-coated perfluorocar-bon nanoemulsions as a sono-photoacoustic contrast agent. *Nano Lett*. 2017;17(10):6184–6194. doi:10.1021/acs.nanolett.7b02845

19. Fernandes DA, Kolios MC. Near-infrared absorbing nanoemulsions as nonlinear ultrasound contrast agents for cancer theranostics. *J Mol Liq*. 2019;287:110848. doi:10.1016/j.molliq.2019.04.125

20. Santiesteban DY, Hallam KA, Yarmoska SK, Emelianov SY. Color-coded perfluorocarbon nanodroplets for multiplexed ultrasound and photoacoustic imaging. *Nano Res*. 2019;12(4):741–747. doi:10.1007/ s12274-019-2279-x

21. Tang W, Yang Z, Wang S, et al. Organic semiconducting photoacous-tic nanodroplets for laser-activatable ultrasound imaging and combi-national cancer therapy. *ACS Nano*. 2018;12(3):2610–2622. doi:10.1021/acsnano.7b08628

22. Lu N, Fan W, Yi X, et al. Biodegradable hollow mesoporous orga-nosilica nanotheranostics for mild hyperthermia-induced bubble-enhanced oxygen-sensitized radiotherapy. *ACS Nano*. 2018;12(2):1580–1591. doi:10.1021/acsnano.7b08103

23. Liu W, Liu S, Liou Y, et al. Nanodroplet-vaporization-assisted sono-poration for highly effective delivery of photothermal treatment. *Sci Rep*. 2016;6:24753. doi:10.1038/srep24753

24. Liu WW, Huang SH, Li PC. Synchronized optical and acoustic droplet vaporization for effective sonoporation. *Pharmaceutics*. 2019;11(6):279. doi:10.3390/pharmaceutics11060279

25. Ho Y, Yeh C. Theranostic performance of acoustic nanodroplet vaporization-generated bubbles in tumor intertissue. *Theranostics*. 2017;7(6):1477–1488. doi:10.7150/thno.19099

26. Fan C, Lin Y, Ho Y, Yeh C. Spatial-temporal cellular bioeffects from acoustic droplet vaporization. *Theranostics*. 2018;8(20):5731–5743. doi:10.7150/thno.28782

27. Qin D, Zhang L, Chang N, et al. In situ observation of single cell response to acoustic droplet vaporization: membrane deformation, permeabilization, and blebbing. *Ultrason Sonochem*. 2018;47:141–150. doi:10.1016/j.ultsonch.2018.02.004

28. Huynh E, Zheng G. Engineering multifunctional nanoparticles: all-in-one versus one-for-all. *Wiley Interdiscip Rev Nanomed Nanobiotechnol*. 2013;5(3):250–265. doi:10.1002/wnan.1217

29. Roper DK, Ahn W, Hoepfner M. Microscale heat transfer transduced by surface plasmon resonant gold nanoparticles. *J Phys Chem C*. 2007;111(9):3636–3641. doi:10.1021/jp064341w

30. Bratosin D, Mitrofan L, Palii C, Estaquier J, Montreuil J. Novel fluorescence assay using calcein-AM for the determination of human erythrocyte viability and aging. *Cytometry A*. 2005;66 (1):78–84. doi:10.1002/cyto.a.20152

31. Walter KA, Tamargo RJ, Olivi A, Burger PC, Brem H. Intratumoral chemotherapy. *Neurosurgery*. 1995;37(6):1129–1145. doi:10.1227/ 00006123-199512000-00013

32. Nomura T, Nakajima S, Kawabata K, et al. Intratumoral pharmaco-kinetics and in vivo gene expression of naked plasmid DNA and its cationic liposome complexes after direct gene transfer. *Cancer Res*. 1997;57(13):2681–2686.

33. Xie H, Goins B, Bao A, Wang ZJ, Phillips WT. Effect of intratu-moral administration on biodistribution of 64Cu-labeled nanoshells. *Int J Nanomedicine*. 2012;7:2227–2238. doi:10.2147/ IJN.S30699

34. Guo Y, Wang X, Chen Y, et al. A light-controllable specific drug delivery nanoplatform for targeted bimodal imaging-guided photo-thermal/chemo synergistic cancer therapy. *Acta Biomater*. 2018;80:308–326. doi:10.1016/j.actbio.2018.09.024

35. Mountford PA, Borden MA. On the thermodynamics and kinetics of superheated fluorocarbon phase-change agents. *Adv Colloid Interface Sci*. 2016;237:15–27. doi:10.1016/j.cis.2016.08.007

36. Kee ALY, Teo BM. Biomedical applications of acoustically respon-sive phase shift nanodroplets: current status and future directions. *Ultrason Sonochem*. 2019;56:37–45. doi:10.1016/j.ultsonch.20 19.03.024

37. Kopechek JA, Park E, Mei C, McDannold NJ, Porter TM. Accumulation of phase-shift nanoemulsions to enhance MR-guided ultrasound-mediated tumor ablation in vivo. *J Healthc Eng*. 2013;4 (1):109–126. doi:10.1260/2040-2295.4.1.109

38. Nyankima AG, Rojas JD, Cianciolo R, Johnson KA, Dayton PA. In vivo assessment of the potential for renal bio-effects from the vaporization of perfluorocarbon phase-change contrast agents. *Ultrasound Med Biol*. 2018;44(2):368–376. doi:10.1016/j. ultrasmedbio.2017.10.016

39. Zha Z, Yue X, Ren Q, Dai Z. Uniform polypyrrole nanoparticles with high photothermal conversion efficiency for photothermal ablation of cancer cells. *Adv Mater*. 2013;25(5):777–782. doi:10.1002/ adma.201202211

40. Wang S, Zhou Z, Yu G, et al. Gadolinium metallofullerene-polypyrrole nanoparticles for activatable dual-modal imaging-guided photothermal therapy. *ACS Appl Mater Interfaces*. 2018;10(34):28382–28389. doi:10.1021/acsami.8b09670

41. Wang X, Ma Y, Sheng X, Wang Y, Xu H. Ultrathin polypyrrole nanosheets via space-confined synthesis for efficient photothermal therapy in the second near-infrared window. *Nano Lett*. 2018;18 (4):2217–2225. doi:10.1021/acs.nanolett.7b04675

42. Zhao Y, Song W, Wang D, et al. Phase-shifted PFH@PLGA/Fe$_3$O$_4$ nanocapsules for MRI/US imaging and photothermal therapy with near-infrared irradiation. *ACS Appl Mater Interfaces*. 2015;7 (26):14231–14242. doi:10.1021/acsami.5b01873

43. Wang L, Chen S, Zhu Y, et al. Triple-modal imaging-guided chemo-photothermal synergistic therapy for breast cancer with magnetically targeted phase-shifted nanoparticles. *ACS Appl Mater Interfaces*. 2018;10(49):42102–42114. doi:10.1021/acsami.8b16323

44. Mou C, Yang Y, Bai Y, et al. Hyaluronic acid and polydopamine functionalized phase change nanoparticles for ultrasound imaging-guided photothermal-chemotherapy. *J Mater Chem B*. 2019;7(8):1246–1257. doi:10.1039/C8TB03056A

45. Fix SM, Novell A, Yun Y, Dayton PA, Arena CB. An evaluation of the sonoporation potential of low-boiling point phase-change ultrasound contrast agents in vitro. *J Ther Ultrasound*. 2017;5(1):7. doi:10.1186/s40349-017-0085-z

46. Feng Y, Qin D, Zhang J, et al. Occlusion and rupture of ex vivo capillary bifurcation due to acoustic droplet vaporization. *Appl Phys Lett*. 2018;112(23):233701. doi:10.1063/1.5025594

47. Seda R, Li DS, Fowlkes JB, Bull JL. Characterization of bioeffects on endothelial cells under acoustic droplet vaporization. *Ultrasound Med Biol*. 2015;41(12):3241–3252. doi:10.1016/j. ultrasmedbio.2015.07.019

48. Shamout FE, Pouliopoulos AN, Lee P, et al. Enhancement of non-invasive trans-membrane drug delivery using ultrasound and microbubbles during physiologically relevant flow. *Ultrasound Med Biol*. 2015;41(9):2435–2448. doi:10.1016/j.ultrasmedbio.2015.05.003

49. Zhang L, Wang D, Yang K, et al. Mitochondria-targeted artificial "nano-RBCs" for amplified synergistic cancer phototherapy by a single NIR irradiation. *Adv Sci*. 2018;5(8):1800049. doi:10.1002/ advs.201800049

50. Zhang C, Liu J, Guo H, et al. Theranostic nanomedicine carrying L-menthol and near-infrared dye for multimodal imaging-guided photothermal therapy of cancer. *Adv Healthcare Mater*. 2019;8 (16):1900409. doi:10.1002/adhm.201900409

51. Chen H, Brayman AA, Bailey MR, Matula TJ. Blood vessel rupture by cavitation. *Urol Res*. 2010;38(4):321–326. doi:10.1007/s00240-010-0302-5

52. Ho YJ, Chang YC, Yeh CK. Improving nanoparticle penetration in tumors by vascular disruption with acoustic droplet vaporization. *Theranostics*. 2016;6(3):392–403. doi:10.7150/thno.13727